Title

Structural and Optical Interplay of Palladium-Modified TiO2 Nanoheterostructure

Journal

The Journal of Physical Chemistry C, 119(4)

ISSN

1932-7447

Authors

Li, Jun

Sham, Tsun-Kong

Ye, Yifan

et al.

Publication Date

2015-01-29

DOI

10.1021/jp511080q

Peer reviewed

Structural and Optical Interplay of Palladium Modified TiO_2 Nano-heterostructure

Jun Li,[a] *Tsun-Kong Sham,*[a]* *Yifan Ye,*[b,c] *Junfa Zhu,*[c] *Jinghua Guo*[b]

[a] Department of Chemistry, University of Western Ontario, 1151 Richmond Street, London, Ontario N6A5B7, Canada.

[b] Advanced Light Source, Lawrence Berkeley National Laboratory, Berkeley, California 94720, United States

[c] National Synchrotron Radiation Laboratory and Collaborative Innovation Center of Suzhou Nano Science and Technology, University of Science and Technology of China, Hefei, Anhui 230029, People's Republic of China

ABSTRACT

The electronic structure and optical properties of Pd modified TiO_2 nanotubes (NTs) with vertically aligned nanotubular structure grown by a two-step electrochemical anodization method have been studied using X-ray spectroscopy. X-ray Absorption Near Edge Structure (XANES) at Ti $L_{3,2}$- and O K-edge has been used to investigate the TiO_2 NTs before and after Pd modification. It is found that Pd nanoparticles (NPs) are uniformly coated on the NTs' surface. Pd L_3-edge of the deposited Pd NPs shows a more intense whiteline and a blue shift for the Pd

L_3-edge absorption threshold relative to Pd metal, indicating charge-depletion from Pd 4d orbital as a result NP formation. The lattice of Pd is slightly contracted upon NP formation albeit it remains fcc as revealed from the Extended X-ray Absorption Fine Structure (EXAFS) analysis at the Pd K-edge. X-ray Excited Optical Luminescence (XEOL) together with XANES with element and site specificity is used to study the optical luminescence from TiO_2 NTs. It is found that the defect-originated XEOL intensity drops noticeably in the Pd NPs coated NTs, suggesting a Pd NP-TiO_2 interaction mediated reduction in the radiative recombination of electrons and holes. Further evidence is provided by Ti 2p resonant inelastic X-ray scattering (RIXS) in which no low energy loss features (d-d transition) are observed. The implications of these results are discussed.

KEYWORDS. electronic structure, X-ray absorption near edge structure, extended X-ray absorption fine structure, X-ray excited optical luminescence, resonant inelastic X-ray scattering.

INTRODUCTION

As arguably one of the most versatile semiconductors, TiO_2 has drawn a great deal of attentions due to its low-cost, non-toxic and superior photocatalytic properties among many other desirable properties. These properties of TiO_2 make it a robust material for solar cells,[1-3] and photocatalysis[4-6] applications among many others.[7-13] Particularly, one-dimensional (1D) TiO_2 nanomaterials, such as nanowires (NWs), nanorods (NRs), nanobelts (NBs) and nanotubes (NTs) are of great scientific interests due to their unique architecture and associated intrinsic properties which can effectively improve photocatalytic efficiency.[14-15] Of the above mentioned morphologies, TiO_2 NTs have been widely used as the effective 1D nanostructure to enhance photocatalytic property of TiO_2. This is because the nanotubular structure can facilitate electron mobility along the tube axis, thus greatly reducing interface recombination.[16] However, the intrinsic defects (e.g., oxygen vacancies) within crystalline TiO_2 NTs impose significant restrictions on their photocatalytic performance. Recently, construction of TiO_2 NTs-based heterojunctions with noble metals attract great attention in photocatalysis, of which systems using silver, gold and platinum achieve the greatest success.[17-19] The reason is that once the TiO_2 absorbs light and produces electrons and holes, the involvement of noble metals which have great electron affinity will be the electron trap sites, thus retarding the recombination of excited electron-hole pairs to mediate photocatalytic performance. In addition, palladium, as another noble metal, has been widely used as an industrial photocatalyst. For example, the decoration of Pd onto TiO_2 NTs has been founded recently to retard the electron-hole recombination, thus enhancing photocatalysis in water-splitting.[6]

To achieve the synergetic effect between Pd and TiO_2 NTs for the design of efficient photocatalyst, the control of physical and chemical properties of TiO_2 NTs as a substrate is

crucial. Of which the morphology and crystal phase of TiO_2 NTs are the top two key factors for Pd modification and photocatalysis performance. While TiO_2 NTs synthesized under conventional techniques like sol-gel[20-21] and hydrothermal method[22-23] suffer the severely morphological limitation (disordered nanostructures and small surface area) resulting in the fast recombination of photoelectrons on the conduction band and holes on the valence band of TiO_2. In contrast, electrochemical anodization, as a productive and growth-controllable synthesis technique of TiO_2 NTs, can grow vertically aligned TiO_2 NTs on Ti substrate in only one direction. These anodic NTs can provide not only well-ordered unidirectional electrical channel but also a large surface area resulting in superior photocatalytic properties.[4-6] Since the photocatalytic performance of TiO_2 NTs is particularly related to its geometry and alignment, TiO_2 NTs with smooth top surface and good nanotubular arrangement are desired to further enhance the photoactivities. However, it is experimentally challenging to obtain the ideal geometry prepared by a single step anodization, in which the ideal NT morphology can be hardly achieved and the disordered architecture severely limits the photocatalytic properties of TiO_2 NTs.[4] Therefore a multi-step anodization method is widely used for TiO_2 NTs growth since the ordered hexagonal imprints can be left behind on Ti substrate after the removal of the previously anodized film. And the following NTs can grow favorably along with these hexagonal imprints, leading to the extremely ordered TiO_2 NTs which show the superior photocatalytic performance and can be used as the ideal substrate for noble metal decoration.[4, 6]

In addition, anatase and rutile are the two well-known and photoactive phases of TiO_2. The different distortions of the octahedral environment at the Ti site result in the local symmetry D_{2d} and D_{2h} for anatase and rutile, respectively. While rutile (density 4.23 g cm^{-3}) is the thermodynamically stable phase, the metastable anatase phase (density 3.78 g cm^{-3}) is the more

preferable phase in nanoscale and possesses an overall lower surface energy, thus anatase is more bioactive and robust for photocatalysis. Usually, the as-prepared TiO_2 NTs have the amorphous structure under room temperature anodization and can be crystallized to different phases (anatase and rutile) using a thermo-controllable method via annealing at different temperatures. The amorphous to anatase transformation temperature, which is greatly dependent on the morphology and defects of TiO_2, varies from 200 ℃ ~ 600 ℃ and a better crystallinity can be achieved using a higher annealing temperature.[24-25] However, the anatase phase will transform to rutile phase if the annealing temperature is too high whence the NTs will collapse and shrink to form the compact rutile structure.[26] Thus the phase control of TiO_2 NTs is a very important issue because different phase can result in a different photo-reaction mechanism. Previous studies indicate that anatase phase of TiO_2 is more stable in closely packed NTs than in loosely packed ones. For example, NTs synthesized by a multi-step anodization can retard the anatase-to-rutile phase transformation temperature to as high as 650℃[4] while NT prepared by single-step anodization shows a noticeable rutile phase and becomes rutile dominant after annealing at 500℃ and 600℃, respectively.[26] Therefore, a multi-step electrochemical anodization method can be used to grow unidirectionally ordered TiO_2 NTs and becomes an easier way to control and retain the anatase phase. The obtained NT structure is highly favorable for Pd modification to achieve a better photocatalytic performance.[6]

It is well documented that the existence of Schottky potential barrier at the interface between Pd NPs (metal) and TiO_2 NTs (semiconductor) facilitates electron transfer from the conduction band of TiO_2 to Pd as the electron affinity of anatase (~4.2 eV)[27] is lower than the work function of Pd (~5.12 eV),[28] which can effectively reduce the electron-hole recombination so that enhanced photoactivity can be achieved.[6, 29] Although many works have been reported to achieve

superior photocatalytic performance of TiO_2 NTs upon Pd decoration,[6, 30-32] to the best of our knowledge, a comprehensive understanding of the synergetic effect between noble metal and TiO_2 is lacking. Thus the objective of this work is to provide insights into electronic structure and its interplay with optical properties of Pd NPs coated TiO_2 NTs.

Investigation of electronic structure using X-ray absorption fine structure (XAFS), which is generally called X-ray absorption spectroscopy (XAS) for short, refers to the modulation of the X-ray absorption coefficient of the core level of the element of interest. Traditionally, XAFS can be divided into X-ray absorption near edge structure (XANES) and extended X-ray absorption fine structure (EXAFS). Of which XANES is a powerful tool to probe the local symmetry and unoccupied electronic states of materials at the near edge region (~20 eV below and ~50 eV above the absorption threshold);[33] EXAFS, on the other hand, can reveal the interatomic distance and coordination number of the site of interest in the materials at the extended absorption region (~50 eV and up to ~1000 eV above the absorption threshold).[34] If the material of interest is light-emitting, then its absorption coefficient modification also can be tracked by the optical yield. Optical photons induced by X-ray absorption is called X-ray excited optical luminescence (XEOL), and can be element and excitation channel specific. [35-36] As a photon-in and photon-out technique, XEOL uses a tunable X-ray source to selectively excite a core level electron and then tracks the energy transfers into optical channels. Absorption across an edge turns on a new Auger channel and will change the thermalization process of the electrons and the holes, of which the radiative recombination is responsible for optical emission. Thus XEOL, in combination with XANES, can reveal the luminescence mechanism of materials with element and site specificity. Resonant inelastic X-ray scattering (RIXS), a complementary tool of XANES, is related to X-ray emission spectroscopy (XES) at resonance in the study of the electronic structure of occupied

states. The concerted dipole transition processes of excitation and de-excitation involved in RIXS makes it an extremely powerful tool for studying the electronic structure of the valence band in the ground state and electronic excitations.[37]

Herein we report the XANES and XEOL studies of TiO_2 NTs prepared under controlled conditions to reveal the synergetic effects of vertically aligned TiO_2 NTs and uniformly coated Pd NPs through the analysis of Ti $L_{3,2}$-edge, O K-edge, Pd L_3- and K-edge as well as related optical luminescence excited by X-rays. In addition, RIXS is also used to pinpoint the effect of Pd modification on the Ti 3d states via d-d transitions analysis.

EXPERIMENTAL SECTION

Highly ordered TiO_2 NTs were prepared by electrochemical anodization using a custom-made two-electrode cell. A Ti metal foil (2 cm × 0.5 cm, 0.1 mm thick, Goodfellow) was used as the anode for NT growth while a Pt wire was the cathode. During the anodic oxidation process, 0.3 wt. % of ammonium fluoride (NH_4F, ACS, 98.0% min, Alfa Aesar) and 2 vol. % of deionized water together with ethylene glycol were used as the electrolyte. In order to grow an ideal nanotubular structure for palladium deposition, a two-step anodization method was used: Ti foil was firstly anodized at 50 V (Hewlett-Packard-6209B DC power supply) for 4 h, and ultrasonically rinsed in 1 M HCl to peel off the first layer. Subsequently, a second anodization was performed at 50 V for 1 h to obtain the vertically aligned NTs. The as-prepared NTs (APNT) attached on Ti foil were crystalized through annealing at 450 ℃ for 2 h (denoted as NT450).

A hydrothermal method[6] was used for palladium modification. Briefly, a 13 ml solution consisting of 150 mg of polyvinylpyrrolidone (PVP, average M_w ~55,000, Sigma-Aldrich), 50 mg of sodium iodide (NaI, ACS reagent, > 99.5%, Sigma-Aldrich) and 1.3 mg of palladium

chloride ($PdCl_2$, ~99%, Sigma-Aldrich) together with NT450 were transferred into a 30 ml Teflon-lined stainless-steel autoclave and then heated at 180 ℃ for 1 h under sealing. Subsequently, the palladium coated NTs (henceforth denoted as PCNT450) were washed with ethanol and dried with N_2 gas.

The morphology of NT450 and PCNT450 was revealed using scanning electron microscopy (SEM, LEO 1540XB), the related SEM images are shown in Figure S1, the vertically aligned NTs have a diameter of ~100 nm with an average wall thickness of ~30 nm. After palladium modification (Figure S1b), the NPs with the diameter of ~10 nm are uniformly deposited on the orifice, the inner and outer tube-wall without changing the morphology of NTs.

The XRD spectra were collected using a Rigaku rotating-anode X-ray diffractometer with Co K_α radiation from 2-82° with a scan rate of $2\theta = 10°$ min^{-1} as shown in Figure S2. Clearly, the structure of the APNT is amorphous, so only diffraction signal from Ti substrate is observed. After annealing at 450℃, NT450 and PCNT450 only present diffraction patterns consistent with anatase phase. A noticeable palladium diffraction peak (200) is located at $2\theta = 55.5°$ in PCNT450 and no other additional Pd peaks are detected, indicating that the size of Pd NPs deposited on the surface of NTs is very small,[6] which is consistent with the SEM result.

XAFS spectra were recorded at the Canadian Light Source (CLS) located at the University of Saskatchewan (Saskatoon, SK, Canada). The Ti $L_{3,2}$-edge and O K-edge were obtained on the Spherical Grating Monochromator (SGM, $E/\Delta E > 5000$) beamline.[38] Pd L_3-edge was measured on the Soft X-Ray Microcharacterization Beamline (SXRMB, $E/\Delta E > 5000$)[39] while Pd K-edge was collected on the Hard X-ray MicroAnalysis (HXMA, $E/\Delta E > 5000$) beamline.[40] The surface-sensitive total electron yield (TEY) and bulk-sensitive fluorescence yield (FLY) were used for absorption spectra collection. An Ocean Optics QE 65000 spectrometer was used for tracking

XEOL spectra during the XAFS spectra collection (i.e., XAFS and XEOL were measured simultaneously by using different detectors). Photoluminescence yield (PLY), as a reflection of XEOL intensity variation which is also treated as optical-XANES, was tracked as the excitation energy tuned from below to above the edge of interest. All spectra were normalized to the incident photon flux. The resonant inelastic X-ray scattering (RIXS) spectra of NT450 and PCNT450 were collected at beamline 8.0.1 at the Advanced Light Source (ALS), Lawrence Berkeley National Laboratory (LBNL). Ti 2p RIXS spectra were measured using a high-resolution grazing incidence grating spectrometer with a resolution of 0.4 eV.[41]

RESULTS AND DISCUSSION

The effect of Pd decoration to the electronic structure of TiO_2 NTs substrate can be revealed by the investigation of Ti $L_{3,2}$-edge and O K-edge as shown in Figure 1, in which the XANES spectra of commercial anatase and rutile (*Sigma-Aldrich*) are used as standards for comparison. Fine structures at Ti $L_{3,2}$-edge arise from transitions from $2p_{3/2}$ and $2p_{1/2}$ to unoccupied $3d_{5/2}$ and $3d_{3/2}$ states of Ti site according to the dipole selection rule ($\Delta l = \pm 1$, $\Delta j = 0, \pm 1$). From Figure 1a, several resonances are presented in the TEY spectra of all samples: two weak pre-edge peaks (p_1 and p_2), two L_3 characteristic peaks t_1 and e_1 (further splitting into e_{11} and e_{12}) and two L_2 characteristic peaks t_2 and e_2. Of which the origin of pre-edge feature p_1 and p_2 is multiplet splitting due to core hole-d electron interactions.[42-43] The energy region from 457.5 to 462 eV is the L_3-edge, peak t_1 and e_1 are transitions to t_{2g} and e_g states, respectively.[44] A further splitting of the second peak of L_3-edge (e_1) into e_{11} and e_{12} is due to the local distortion at the Ti site from the octahedron (O_h) structure.[45] The relative intensity of e_{11} and e_{12} can be used to distinguish between the anatase and rutile crystal structure of TiO_2. The higher intensity of e_{11} over e_{12} as

shown in Figure 1a indicates that anatase (D_{2d} symmetry) is the dominant structure in NT450 and PCNT450,[26, 45] which is also in good accordance with the XANES profile of standard anatase sample presented in Figure 1a.

The energy region from 462 to 470 eV is the L_2-edge region, and peak t_2 and e_2 are transitions to t_{2g} and e_g states, respectively.[44] Compared with the e_1 peak splitting at L_3-edge, however, we cannot find e_2 peak splitting in this L_2-edge region which is partly due to the life-time broadening (core-hole effect) because of Coster-Kronig transitions and partly due to the interference of L_3-edge EXAFS underneath. The non-splitting e_1 feature, together with the shorter energy distance between t_2 and e_2, of APNT is due to its amorphous structure, which is consistent with XRD result and previous studies.[26, 45]

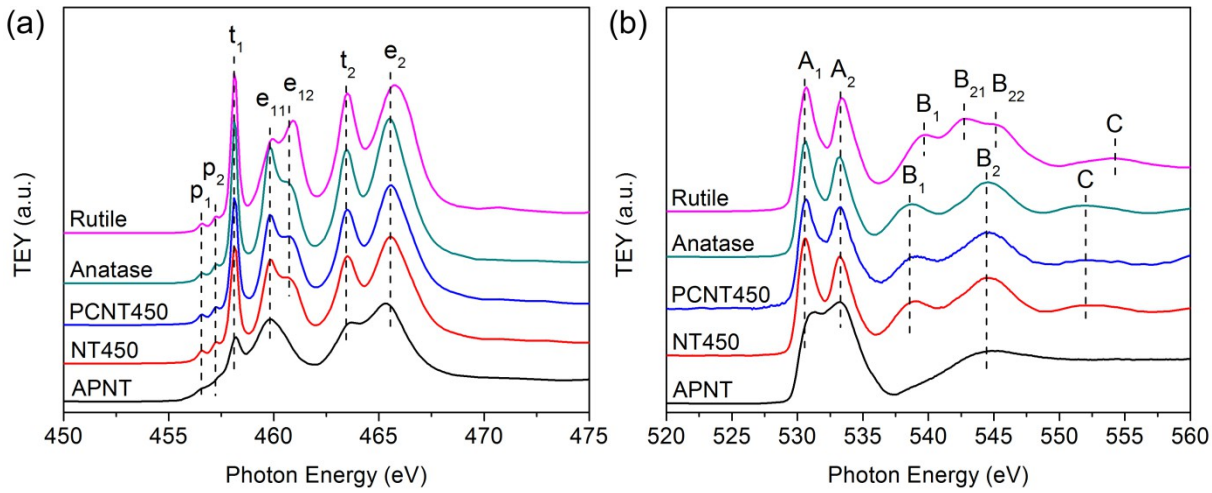

Figure 1. (a) Ti $L_{3,2}$-edge and (b) O K-edge XANES spectra of APNT, NT450, PCNT450, commercial anatase and rutile (*Sigma-Aldrich*); All spectra are normalized to the edge jump (flat region of the absorption above the threshold); All except the APNT are shifted vertically for clarity.

Fine structures at the O K-edge (Figure 1b) arise from dipole transitions from 1s to unoccupied 2p states of O site; different types of features presented in Figure 1b are due to transitions to the hybridized states between O 2p and Ti 3d or Ti 4sp: The pre-edge within energy region from 529 to 536 eV is transition from O 1s to unoccupied O 2p-Ti 3d hybridized states.[45] And the splitting into two intense peak A_1 and A_2 is due to splitting of Ti 3d band and transitions to t_{2g} and e_g states, respectively, which, as a common feature in transitional metal oxides, clearly shows the strong hybridization between O 2p and Ti 3d orbitals. Peaks B_1 and B_2 are transitions from O 1s to O 2p-Ti 4sp hybridized bands while the appearance of higher energy resonance peak C located at ~553eV reflects the long range order in these crystalline samples. It is worth noting that the further peak splitting of B_2 into B_{21} and B_{22} together with energy shifts of peak B_1 and C indicates the totally different local environment of O site in rutile phase (D_{2h} symmetry) compared to anatase phase (D_{2d} symmetry). Therefore by comparing the O K-edge XANES of anatase and rutile (Figure 1b), we can conclude that both NT450 and PCNT450 display anatase structure by sharing the similar O K-edge XANES spectra pattern. The broad pre-edge feature, together with the absence of peak C, of APNT at the O K-edge indicates its amorphous structure,[26, 45] which is in good accordance with Ti $L_{3,2}$-edge XANES study. Therefore, both the XANES spectra from Ti $L_{3,2}$-edge and O K-edge do not show any noticeable difference before and after Pd modification, indicating Pd NPs in this work are only coated on the surface of NTs.[6, 46]

To provide evidence of Pd NPs coating onto NTs, the study of Pd itself is necessary and the Pd L_3-edge XAFS spectra are shown in Figure 2a. Of which the Pd L_3-edge of Pd foil and $PdCl_2$ (*Sigma-Aldrich*) are shown as standards for comparison. From Figure 2a, the Pd L_3-edge XAFS spectra of PCNT450 and Pd foil have the similar spectral features. The oscillating patterns (peak f to h) are the EXAFS signature of fcc metallic Pd,[47-48] indicating Pd(II) is successfully reduced

to Pd(0). After the reaction, a brown color can be observed in the post-reaction solution which can easily make starch solution turn blue. Thus it shows that I^- is oxidized to I_2 having served as the reducing agent to convert Pd(II) to the Pd nuclei on the surface of TiO_2 NTs and for subsequent Pd NPs growth. This observation is consistent with the result of SEM where Pd NPs are uniformly deposited on the surface of TiO_2 NTs.

In the Pd L_3-edge XANES, the first intense peak, so-called whiteline (WL) appears as a sharp resonance just above the threshold; it arises from $2p_{3/2}$ to 4d states transitions, and the area underneath the WL is proportional to the unoccupied densities of states of the Pd d-band above the Fermi level;[47] i.e., that the larger the area under WL, the higher the unoccupied d-hole count of Pd 4d states, which often correlates to improved catalytic activity. From Figure 2, several interesting observations are noted: First, a significant increase in the WL intensity of $PdCl_2$ and a slightly enhanced WL of PCNT450 relative to Pd foil can be seen (Figure 2a and 2b); Second, compared with the absorption threshold (the first maximum of the first derivative of XANES) of Pd foil (E_0 = 3173 eV), the Pd L_3-edge absorption threshold of PCNT450 and $PdCl_2$ shifts by 0.6 eV and 0.9 eV, respectively, to the higher energy region (Figure 2c). Meanwhile, upon palladium NPs formation, the Pd L_3-edge of PCNT450 shows a noticeable broadening in all resonance peaks than that of Pd foil (Figure 2b). More interestingly, a closer observation within Pd L_3 post-edge region of PCNT450 shows that while peak b slightly shifts to lower energy, all other features (d ~ h) shift with progressive larger separation to the corresponding peaks in Pd metal (the inset of Figure 2b).

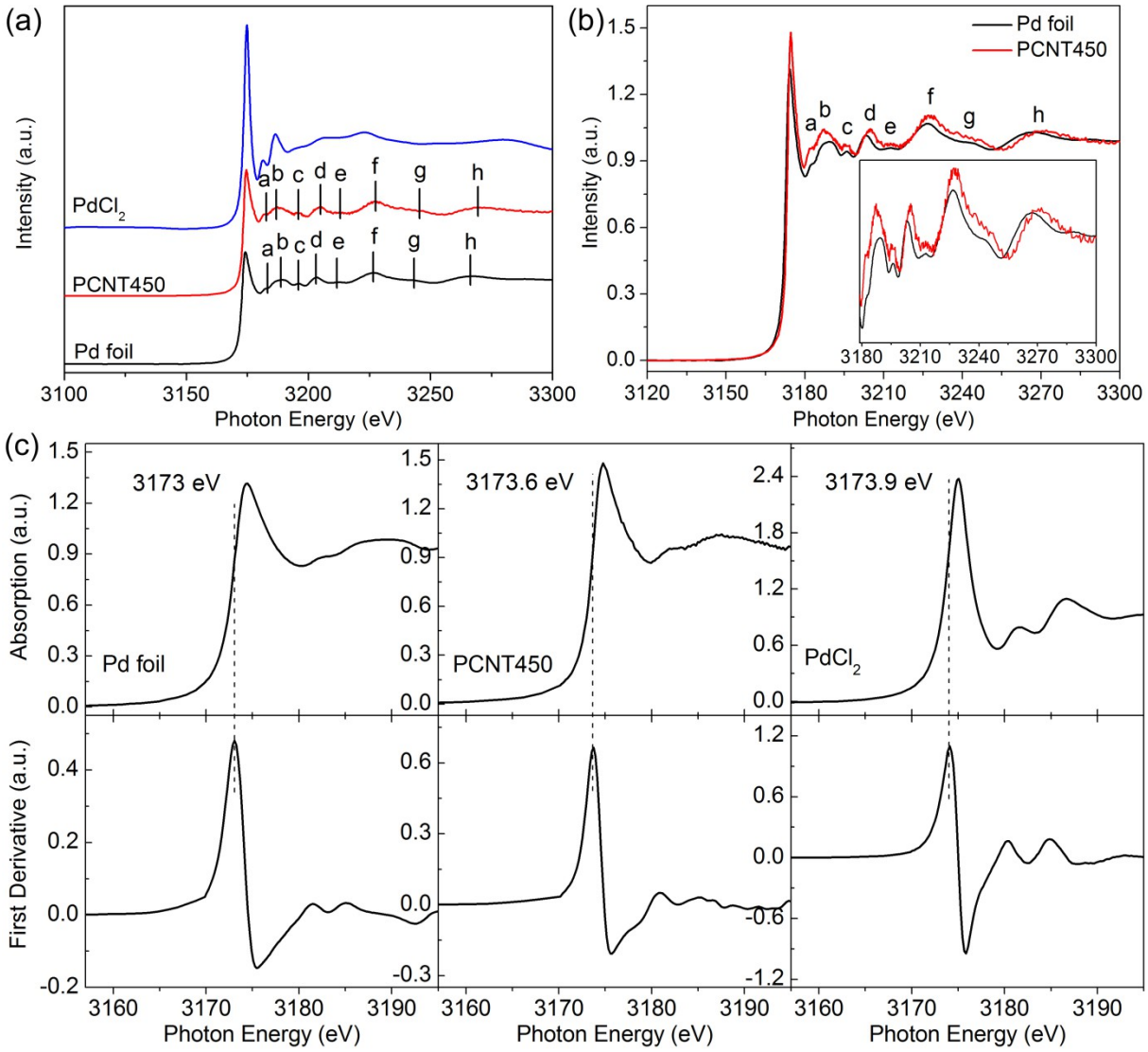

Figure 2. (a) Pd L_3-edge XAFS spectra of Pd foil, PCNT450 and $PdCl_2$; (b) A close Pd L_3-edge comparison between Pd foil and PCNT450, the inset is their post-edge comparison; (c) XANES spectra and their first derivatives near Pd L_3-edge whiteline region of Pd foil, PCNT450 and $PdCl_2$ (the vertical dash lines indicate their absorption threshold (E_0)). All XAFS spectra are normalized to the edge jump.

For $PdCl_2$, together with its high-energy-shifted absorption threshold, the intense WL intensity is mainly due to its expected 4d electron configuration of Pd(II) although covalence will reduce

the total d hole to be less than 2.[49] The enhanced WL and slightly broadened feature of PCNT450 relative to the bulk Pd foil indicate a d-charge depletion in Pd 4d band upon NPs formation, which is consistent with the +0.6 eV shift of its absorption threshold since reduced Pd d-d interaction at the nanoparticle surface due to a reduction in coordination number, and the interaction between Pd and TiO_2 will both contribute to d charge depletion on Pd site. Then a more effective hybridization between d and s, p orbitals of Pd would yield positive threshold shift as 4d charge screens the core hole better than 5s and 5p.[48] The energy-shifted features at the Pd L_3 post-edge can be revealed through K-edge EXAFS analysis (see below) and the shift of these features (d ~ h) to a higher energy region often indicates a shorter Pd-Pd bond distance (contracted fcc structure) in the NP relative to bulk. According to a d-hole count calculation method[50-51] and the 0.36 d-hole count of palladium metal,[47, 49] a 0.38 d-hole count is obtained for PCNT450, which is ~ 5.6 % increase compared to the metal foil.

Further confirmation of Pd decoration on TiO_2 NTs is achieved by the Pd K-edge EXAFS study. The similar XAFS oscillation patterns between PCNT450 and Pd foil (Figure 3a) indicate that they have the same fcc structure. The broadening of the Pd K-edge XANES features (inset of Figure 3a) of PCNT450 compared to the sharp features observed in bulk Pd foil results from the degradation of long-range order and disorder due to the truncation of the lattice for Pd NPs formation (surface), and to some extent the Pd and TiO_2 NT interface. It is worth noting that the oscillation pattern of EXAFS is composed of phase and amplitude, in which the former includes bond length and phase information while the latter provides backscattering amplitude, bond length, and coordination number, etc. Since Fourier transform technique can be used to separate the phase and amplitude, and chemical transferability of phase and amplitude works well between Pd NPs and bulk Pd foil due to their similar systems. Thus the Fourier transform process

of the EXAFS oscillations can be used to obtain the bond length difference from the phase analysis and the relative degree of disorder from the amplitude between PCNT450 and Pd foil.[34, 52] Figure 3b shows the Fourier transform of the EXAFS with k weighting (k range: 2.5-15 $Å^{-1}$ for Pd foil while 2.5-13 $Å^{-1}$ for PCNT450). It is evident that the bond length of the first shell of Pd NPs is smaller than that of bulk Pd foil.

Assuming chemical transferability of the phases and amplitude of Pd NPs and bulk Pd foil, a Fourier back-transform of the first shell from the R space to k space with identical filter window as indicated by two black solid bars (R range: 1.5 - 3.0 Å, the inset of Figure 3b) can be used to obtain the difference of the first shell Pd-Pd interatomic distance. Qualitatively, since $r = (2\pi/\Delta k_{max} - \beta)/2$, where r and k are the bond length and wave vector, respectively. β is a constant for low Z scatterers or in the high k region for Pd where the phase of the backscatterer is nearly linear in k.[34] So the larger the Δk_{max}, the shorter the bond, which is the case for PCNT450, suggesting the shorter Pd-Pd bond length of Pd NPs than the bulk Pd foil. And the reduction in amplitude indicates the disorder structure of Pd NPs due to the truncation of the lattice and the decrease of coordination number at the surface. With an assumption that the phase and the backscattering amplitude of Pd are the same in both Pd NP and Pd metal (a reasonable assumption of chemical transferability), the fitted $\Delta r = 0.14$ Å, which was derived from fitting the phase function of Pd NP (extracted from the filtered Fourier back-transform of the first Pd-Pd shell) with that of the Pd metal with a known first shell Pd-Pd distance of 2.75 Å. Intuitively, the fitting result is a little large and it is, probably, due to the partially oxidized shell of Pd NP, resulting in the increase of electron density on the surface and shrinkage of the Pd NP. Because electron transfer from the central Pd atoms to the surface Pd atoms will strength the hybridization between two Pd atoms, thus decreasing the bond distance of Pd-Pd.

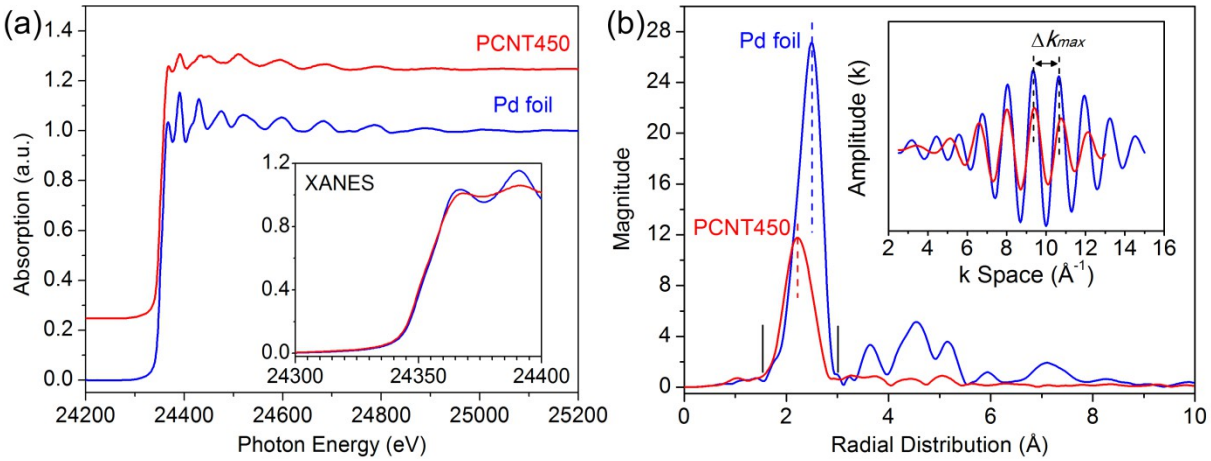

Figure 3. (a) Pd K-edge XAFS of PCNT450 and Pd foil (the PCNT450 spectrum is vertically shifted for comparison); the inset is the Pd K-edge XANES. (b) Fourier transform of the EXAFS for PCNT450 and Pd foil; Note that the bond length difference cannot be directly read off since the Pd backscatter phase is not linear in k space; the inset shows the Fourier back transform with a filter window at the first shell (R range: 1.5-3.0 Å).

Hence, it is no doubt that the obtained Pd NPs coating on TiO_2 NTs show the typical fcc but contracted crystal structure. And the consequent increase of Pd 4d hole count upon NPs formation should be responsible for the superior photoactivity of Pd/TiO_2 heterostructure in water-splitting.[6]

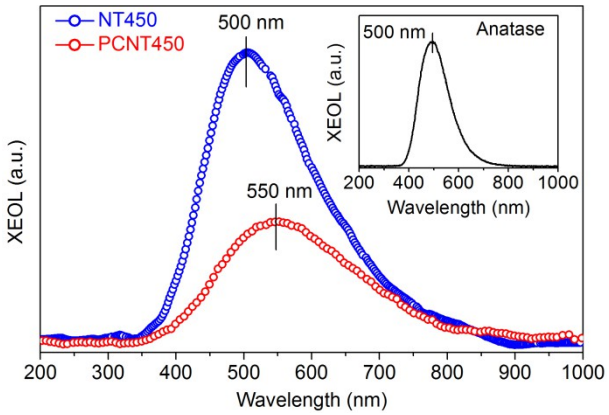

Figure 4. XEOL spectra of NT450 and PCNT450 collected with excitation photon energy at 575 eV normalized to incident flux (well above O K-edge, the inset is the XEOL spectrum of commercial anatase collected at 575 eV).

The effect of palladium coating to the optical property of TiO_2 NTs can be observed with XEOL as shown in Figure 4, in which NT450, like commercial anatase sample, exhibits one broad luminescence band centered at ~500 nm while the wavelength of green emission band shifts to ~550 nm in PCNT450 with a comparatively sharp reduction in its intensity. A thorough luminescence mechanism revelation for these two green emission bands is fully discussed in the supporting information (DISCUSSION and Figure S3). Surface defects of anatase are mainly contributed to the observed luminescence of NT450 and PCNT450, which is consistent with a previous XANES and XEOL study of pure NTs[26] and photoluminescence (PL) studies of Pd modified TiO_2.[53-55] The red shift of PCNT450 XEOL spectrum, compared with the XEOL spectra of NT450 and commercial anatase, is almost certainly due to the surface modification of TiO_2 NTs upon Pd coating. The sharp decrease of XEOL intensity of PCNT450 indicates the reduction of surface defects of anatase by either healing upon Pd NPs coating[46] or suppressing with the preferred deposition of Pd NPs on such surface sites. And the absorption of incident photon by

Pd which does not contribute directly to energy transfer to the optical channel. It should be noted that in pure anatase NTs, photo-excited electrons can be trapped by the surface defects. For Pd modified NTs, on one hand, the photo-generated electrons at TiO_2 conduction band can recombine with valence holes via surface defects which is similar to the recombination process of pure NTs; on the other hand, they can be captured by Pd site at the interface between Pd and TiO_2 since the equalized Femi energy level of PCNT450 (once Pd and TiO_2 are in contact, their Fermi level will equalize and a subsequent Schottky barrier layer will be formed at their interface) is still lower than the energy level of the conduction band of TiO_2. Thus electrons on the conduction band of TiO_2 prefer to transfer to the Pd site, indicating that Pd can act as the electron sink on the surface of TiO_2, hence effectively slowing down the recombination rate of radiative recombination of electrons and holes.

Resonant inelastic X-ray scattering (RIXS) spectroscopy (or RXES) is also used to pinpoint the effect of Pd modification to the Ti 3d states of anatase TiO_2 NTs as shown in Figure 5. The energy loss (Figure 5b) scale is obtained via subtracting the measured emission energy from the excitation energy. Earlier Ti 2p RIXS studies of TiO_2 have been well-established via experimental[37, 41, 56] and theoretical[57] analysis. And it is well documented that three components are included in Ti 2p RIXS (shown in Figure 5b):[41, 58] normal Ti 3d→Ti 2p emissions at fixed photon emission energy (the energy loss scale of these peaks vary as the excitation energy increases and are proportional to the change of the excitation energy) are indicated by the short solid bars; elastic scattering features (which have emission energies equal to the excitation energies) are located at the 0 eV on the energy loss scale; and inelastic scattering features such as charge-transfer features which are shown as constant energy loss peaks (c_1, c_2 and c_3) are located between elastic scattering features and normal Ti 3d→Ti 2p emission peaks. The origin of some

weak energy loss features located between 0 eV and 5 eV below the excitation energy is quite interesting and can be assigned to d-d transitions as inelastic scattering features (shake-up).[41, 58] In Figure 5b, these d-d transition features are clearly presented in NT450 especially when the excitation energy reaches the t_{2g}-resonance (spectrum a and c) and e_g-resonance (spectrum e and f), which, to the best of our knowledge, have not been reported before in Ti 2p RIXS spectra of both pure anatase and rutile TiO_2 nanomaterials. And all these energy loss features are totally quenched upon palladium modification. Previous Ti 2p RIXS study of lithium doped nanoporous anatase TiO_2[41] and $La_xSr_{1-x}TiO_3$[58] indicate that the presence of d-d transition features is due to an extra electron localized at the Ti t_{2g} states, i.e., t_{2g} states are partially occupied instead of the Ti 3d(0) configuration of TiO_2. Therefore, we can attribute the origins of these inelastic scattering features to the reduction of Ti(IV) to Ti(III) (Ti d band is no longer empty) resulting from the defects presented in NT450. More interestingly, the disappearance of these low energy loss features in PCNT450 clearly indicates the coated Pd NPs can effectively heal the defects, especially defects at the interface between Pd and TiO_2, to decrease the recombination probability of photo-excited electron-hole pairs. Thus decoration of Pd NPs onto TiO_2 NTs can efficiently elongate the lifetime of photoactive electron-hole pairs, which is consistent with the XEOL reduction of PCNT450.

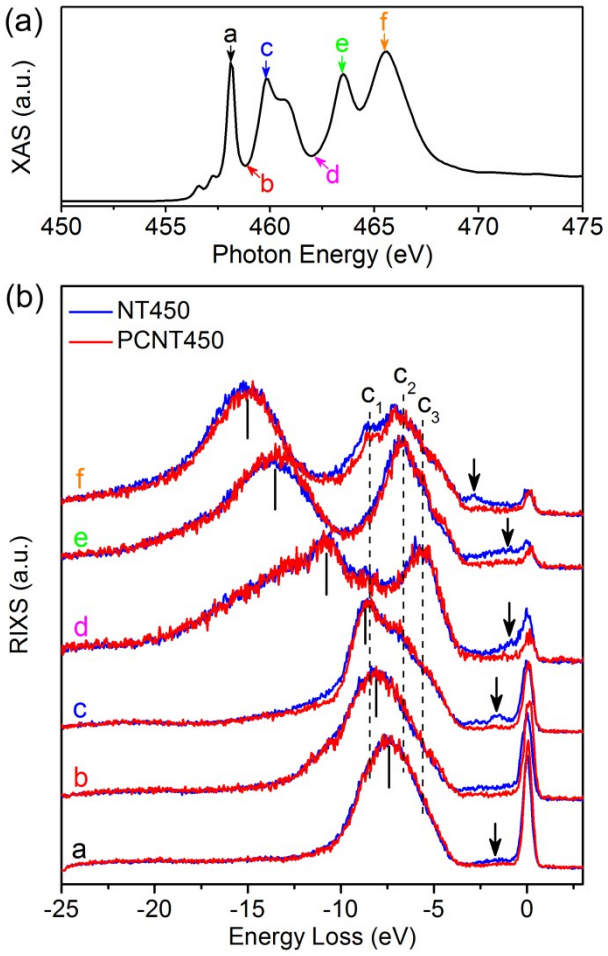

Figure 5. (a) Ti 2p XANES; (b) Ti 2p RIXS spectra of NT450 and PCNT450 excited at the photon energies indicated in the XANES spectrum and each pair RIXS spectra of NT450 and PCNT450 are normalized to their corresponding Ti 3d→Ti 2p emission (indicated by solid bars), respectively. The elastic peak is at 0 energy loss.

CONCLUSIONS

Vertically well-aligned TiO_2 NTs are obtained using a two-step electrochemical anodization process, this ideal nanotubular morphology favors the uniform deposition of Pd NPs on the surface of NTs (inner and outer tube-wall). Several findings are highlighted here: (1) Pd NPs are

only coated on NTs without the noticeable change of electronic structure of pure NTs via Ti $L_{3,2}$- and O K-edge analysis; (2) Pd NP is contracted compared to Pd metal; (3) The sharp reduction of XEOL intensity of Pd modified NTs compared with pure NTs, together with RIXS analysis, indicates that the coated Pd NPs can partially heal the surface defects of anatase. And Pd can remove electrons from the conduction band to efficiently hamper the radiative recombination process.

ASSOCIATED CONTENT

Supporting Information. Page S1: SEM images of NT450 and PCNT450; S2: XRD spectra of APNT, NT450 and PCNT450, and PLY-XANES spectra of NT450 and PCNT450 at Ti $L_{3,2}$-edge and O K-edge. S3-S4: Discussion of luminescence mechanism for the green emission bands of NT450 and PCNT450. This material is available free of charge via the Internet at http://pubs.acs.org.

AUTHOR INFORMATION

Corresponding Author

*E-mail: tsham@uwo.ca.

Notes

The author declares no competing financial interest.

ACKNOWLEDGEMENTS

Research at the University of Western Ontario is supported by NSERC, CRC (TKS), CFI, and OIT. The work at Canadian Light Source (CLS) is supported by CFI, NSERC, NRC, CIHR, and

the University of Saskatchewan. The author (Jun Li) acknowledges the receipt of support from the CLS Graduate Student Travel Support Program. The work at Advanced Light Source is supported by the U.S. Department of Energy at Lawrence Berkeley National Laboratory. We thank Dr. Tim Goldhawk and Dr. Todd Simpson of Nanofabrication Laboratory, University of Western Ontario for SEM characterization, and thank Dr. Grace Yau in the Department of Earth Science, University of Western Ontario for XRD characterization. We also thank Dr. Yongfeng Hu for technical support at the SXRMB beamline, Dr. Ning Chen for technical support at the HXMA beamline, Dr. Tom Regier for technical support at the SGM beamline, Canadian Light Source, and Dr. Wanli Yang for technical support at the beamline 8.0.1, Advanced Light Source.

REFERENCES

1. Yan, J. F.; Zhou, F. TiO_2 Nanotubes: Structure Optimization for Solar Cells. *J. Mater. Chem.* **2011**, *21*, 9406–9418.

2. Mor, G. K.; Shankar, K.; Paulose, M.; Varghese, O. K.; Grimes, C. A. Use of Highly-Ordered TiO_2 Nanotube Arrays in Dye-Sensitized Solar Cells. *Nano Lett.* **2006**, *6*, 215–218.

3. Tian, Z. R. R.; Voigt, J. A.; Liu, J.; McKenzie, B.; Xu, H. F. Large Oriented Arrays and Continuous Films of TiO_2-Based Nanotubes. *J. Am. Chem. Soc.* **2003**, *125*, 12384–12385.

4. Gong, J. J.; Lai, Y. K.; Lin, C. J. Electrochemically Multi-Anodized TiO_2 Nanotube Arrays for Enhancing Hydrogen Generation by Photoelectrocatalytic Water Splitting. *Electrochim. Acta* **2010**, *55*, 4776–4782.

5. Gong, J. J.; Lin, C. J.; Ye, M. D.; Lai, Y. K. Enhanced Photoelectrochemical Activities of A Nanocomposite Film with A Bamboo Leaf-Like Structured TiO_2 Layer on TiO_2 Nanotube Arrays. *Chem. Commun.* **2011**, *47*, 2598–2600.

6. Ye, M. D.; Gong, J. J.; Lai, Y. K.; Lin, C. J.; Lin, Z. Q. High-Efficiency Photoelectrocatalytic Hydrogen Generation Enabled by Palladium Quantum Dots-Sensitized TiO_2 Nanotube Arrays. *J. Am. Chem. Soc.* **2012**, *134*, 15720–15723.

7. Li, Z. Y.; Zhang, H. N.; Zheng, W.; Wang, W.; Huang, H. M.; Wang, C.; MacDiarmid, A. G.; Wei, Y. Highly Sensitive and Stable Humidity Nanosensors Based on LiCl Doped TiO_2 Electrospun Nanofibers. *J. Am. Chem. Soc.* **2008**, *130*, 5036–5037.

8. Shrestha, N. K.; Macak, J. M.; Schmidt-Stein, F.; Hahn, R.; Mierke, C. T.; Fabry, B.; Schmuki, P. Magnetically Guided Titania Nanotubes for Site-Selective Photocatalysis and Drug Release. *Angew. Chem. Int. Ed.* **2009**, *48*, 969–972.

9. Song, Y. Y.; Schmidt-Stein, F.; Bauer, S.; Schmuki, P. Amphiphilic TiO_2 Nanotube Arrays: An Actively Controllable Drug Delivery System. *J. Am. Chem. Soc.* **2009**, *131*, 4230–4232.

10. Balaur, E.; Macak, J. M.; Tsuchiya, H.; Schmuki, P. Wetting Behaviour of Layers of TiO_2 Nanotubes with Different Diameters. *J. Mater. Chem.* **2005**, *15*, 4488–4491.

11. Caramori, S.; Cristino, V.; Argazzi, R.; Meda, L.; Bignozzi, C. A. Photoelectrochemical Behavior of Sensitized TiO_2 Photoanodes in An Aqueous Environment: Application to Hydrogen Production. *Inorg. Chem.* **2010**, *49*, 3320–3328.

12. Mun, K. S.; Alvarez, S. D.; Choi, W. Y.; Sailor, M. J. A Stable, Label-Free Optical Interferometric Biosensor Based on TiO_2 Nanotube Arrays. *ACS Nano* **2010**, *4*, 2070–2076.

13. Zou, J. P.; Zhang, Q.; Huang, K.; Marzari, N. Ultraviolet Photodetectors Based on Anodic TiO_2 Nanotube Arrays. *J. Phys. Chem. C* **2010**, *114*, 10725–10729.

14. Shin, K.; Il Seok, S.; Im, S. H.; Park, J. H. CdS or CdSe Decorated TiO_2 Nanotube Arrays from Spray Pyrolysis Deposition: Use in Photoelectrochemical Cells. *Chem. Commun.* **2010**, *46*, 2385–2387.

15. Hensel, J.; Wang, G. M.; Li, Y.; Zhang, J. Z. Synergistic Effect of CdSe Quantum Dot Sensitization and Nitrogen Doping of TiO_2 Nanostructures for Photoelectrochemical Solar Hydrogen Generation. *Nano Lett.* **2010**, *10*, 478–483.

16. Yan, J. F.; Zhou, F. TiO_2 Nanotubes: Structure Optimization for Solar Cells. *J. Mater. Chem.* **2011**, *21*, 9406–9418.

17. Li, H. B.; Duan, X. C.; Liu, G. C.; Liu, X. Q. Photochemical Synthesis and Characterization of Ag/TiO_2 Nanotube Composites. *J. Mater. Sci.* **2008**, *43*, 1669–1676.

18. Li, X. H.; Chen, G. Y.; Yang, L. B.; Jin, Z.; Liu, J. H. Multifunctional Au-Coated TiO_2 Nanotube Arrays as Recyclable SERS Substrates for Multifold Organic Pollutants Detection. *Adv. Funct. Mater.* **2010**, *20*, 2815–2824.

19. Lin, C. H.; Lee, C. H.; Chao, J. H.; Kuo, C. Y.; Cheng, Y. C.; Huang, W. N.; Chang, H. W.; Huang, Y. M.; Shih, M. K. Photocatalytic Generation of H_2 Gas from Neat Ethanol over Pt/TiO_2 Nanotube Catalysts. *Catal. Lett.* **2004**, *98*, 61–66.

20. Zhang, M.; Bando, Y.; Wada, K. Sol-Gel Template Preparation of TiO_2 Nanotubes and Nanorods. *J. Mater. Sci. Lett.* **2001**, *20*, 167–170.

21. Kobayashi, S.; Hamasaki, N.; Suzuki, M.; Kimura, M.; Shirai, H.; Hanabusa, K. Preparation of Helical Transition-Metal Oxide Tubes Using Organogelators as Structure-Directing Agents. *J. Am. Chem. Soc.* **2002**, *124*, 6550–6551.

22. Chen, Q.; Zhou, W. Z.; Du, G. H.; Peng, L. M. Trititanate Nanotubes Made Via A Single Alkali Treatment. *Adv. Mater.* **2002**, *14*, 1208–1211.

23. Yao, B. D.; Chan, Y. F.; Zhang, X. Y.; Zhang, W. F.; Yang, Z. Y.; Wang, N. Formation Mechanism of TiO_2 Nanotubes. *Appl. Phys. Lett.* **2003**, *82*, 281–283.

24. Zhang, J.; Li, M. J.; Feng, Z. C.; Chen, J.; Li, C. UV Raman Spectroscopic Study on TiO_2. I. Phase Transformation at the Surface and in the Bulk. *J. Phys. Chem. B* **2006**, *110*, 927–935.

25. Ghosh, T. B.; Dhabal, S.; Datta, A. K. On Crystallite Size Dependence of Phase Stability of Nanocrystalline TiO_2. *J. Appl. Phys.* **2003**, *94*, 4577–4582.

26. Liu, L. J.; Chan, J.; Sham, T. K. Calcination-Induced Phase Transformation and Accompanying Optical Luminescence of TiO_2 Nanotubes: An X-Ray Absorption Near-Edge Structures and X-Ray Excited Optical Luminescence Study. *J. Phys. Chem. C* **2010**, *114*, 21353–21359.

27. Ratanatawanate, C.; Tao, Y.; Balkus, K. J. Photocatalytic Activity of PbS Quantum Dot/TiO_2 Nanotube Composites. *J. Phys. Chem. C* **2009**, *113*, 10755–10760.

28. Wang, L.; Nathan, M. I.; Lim, T. H.; Khan, M. A.; Chen, Q. High Barrier Height Gan Schottky Diodes: Pt/GaN and Pd/GaN. *Appl. Phys. Lett.* **1996**, *68*, 1267–1269.

29. Zhang, Z. H.; Yu, Y. J.; Wang, P. Hierarchical Top-Porous/Bottom-Tubular TiO_2 Nanostructures Decorated with Pd Nanoparticles for Efficient Photoelectrocatalytic Decomposition of Synergistic Pollutants. *ACS Appl. Mater. Interfaces* **2012**, *4*, 990–996.

30. Gobal, F.; Faraji, M. Electrodeposited Polyaniline on Pd-Loaded TiO_2 Nanotubes as Active Material for Electrochemical Supercapacitor. *J. Electroanal. Chem.* **2013**, *691*, 51–56.

31. Alexander, M.; Pandian, K. Linen Fiber Template-Assisted Preparation of TiO_2 Nanotubes: Palladium Nanoparticle Coating and Electrochemical Applications. *J. Solid State Electrochem.* **2013**, *17*, 1117–1125.

32. Zhao, R.; Ding, R. F.; Yuan, S. J.; Jiang, W.; Liang, B. Palladium Membrane on TiO_2 Nanotube Arrays-Covered Titanium Surface by Combination of Photocatalytic Deposition and Modified Electroless Plating Processes and Its Hydrogen Permeability. *Int. J. Hydrogen Energy* **2011**, *36*, 1066–1073.

33. De Groot, F. High Resolution X-Ray Emission and X-Ray Absorption Spectroscopy. *Chem. Rev.* **2001**, *101*, 1779–1808.

34. Sun, X. H.; Didychuk, C.; Sham, T. K.; Wong, N. B. Germanium Nanowires: Synthesis, Morphology and Local Structure Studies. *Nanotechnology* **2006**, *17*, 2925–2930.

35. Sham, T. K.; Jiang, D. T.; Coulthard, I.; Lorimer, J. W.; Feng, X. H.; Tan, K. H.; Frigo, S. P.; Rosenberg, R. A.; Houghton, D. C.; Bryskiewicz, B. Origin of Luminescence from Porous Silicon Deduced by Synchrotron-Light-Induced Optical Luminescence. *Nature* **1993**, *363*, 331–334.

36. Sham, T. K.; Naftel, S. J.; Kim, P. S. G.; Sammynaiken, R.; Tang, Y. H.; Coulthard, I.; Moewes, A.; Freeland, J. W.; Hu, Y. F.; Lee, S. T. Electronic Structure and Optical Properties of Silicon Nanowires: A Study Using X-Ray Excited Optical Luminescence and X-Ray Emission Spectroscopy. *Phys. Rev. B* **2004**, *70*.

37. Harada, Y.; Kinugasa, T.; Eguchi, R.; Matsubara, M.; Kotani, A.; Watanabe, M.; Yagishita, A.; Shin, S. Polarization Dependence of Soft-X-Ray Raman Scattering at the L Edge of TiO_2. *Phys. Rev. B* **2000**, *61*, 12854–12859.

38. Regier, T.; Paulsen, J.; Wright, G.; Coulthard, I.; Tan, K.; Sham, T. K.; Blyth, R. I. R. In Commissioning of the Spherical Grating Monochromator Soft X-Ray Spectroscopy Beamline at the Canadian Light Source. *AIP Conf. Proc.* **2007**, *879*, 473–476.

39. Hu, Y. F.; Coulthard, I.; Chevrier, D.; Wright, G.; Igarashi, R.; Sitnikov, A.; Yates, B. W.; Hallin, E. L.; Sham, T. K.; Reininger, R. In Preliminary Commissioning and Performance of the Soft X-Ray Micro-Characterization Beamline at the Canadian Light Source. *AIP Conf. Proc.* **2010**, *1234*, 343–346.

40. Li, J. W.; Chen, X. B.; Matias, E.; Zhang, W. J. Design of Photon Beam Vibration Measurement System for the CLS HXMA Beamline. *Proc. ASME Int. Mech. Eng. Congr. Expo.* **2012**, *13*, 91–99.

41. Augustsson, A.; Henningsson, A.; Butorin, S. M.; Siegbahn, H.; Nordgren, J.; Guo, J. H. Lithium Ion Insertion in Nanoporous Anatase TiO_2 Studied with RIXS. *J. Chem. Phys.* **2003**, *119*, 3983–3987.

42. Henderson, G. S.; Liu, X.; Fleet, M. E. A Ti L-Edge X-Ray Absorption Study of Ti-Silicate Glasses. *Phys. Chem. Miner.* **2002**, *29*, 32–42.

43. Crocombette, J. P.; Jollet, F. Ti 2p X-Ray-Absorption in Titanium Dioxides (TiO_2) - the Influence of the Cation Site Environment. *J. Phys.: Condens. Matter* **1994**, *6*, 10811–10821.

44. Li, T.; Larciprete, R.; Turchini, S.; Zema, N.; Bonanni, A.; Di Trolio, A. Substrate-Driven Formation of Bidimensional Arrays of Co Nanocrystals in TiO_2 Thin Films. *J. Phys. Chem. C* **2013**, *117*, 687–691.

45. Zhou, J. G.; Fang, H. T.; Maley, J. M.; Murphy, M. W.; Ko, J. Y. P.; Cutler, J. N.; Sammynaiken, R.; Sham, T. K.; Liu, M.; Li, F. Electronic Structure of TiO_2 Nanotube Arrays from X-Ray Absorption Near Edge Structure Studies. *J. Mater. Chem.* **2009**, *19*, 6804–6809.

46. Chang, Y. G.; Xu, J.; Zhang, Y. Y.; Ma, S. Y.; Xin, L. H.; Zhu, L. N.; Xut, C. T. Optical Properties and Photocatalytic Performances of Pd Modified ZnO Samples. *J. Phys. Chem. C* **2009**, *113*, 18761–18767.

47. Sham, T. K. L-Edge X-Ray-Absorption Spectra of $PdAl_3$ and $PdCl_2$ - A Study of Charge Redistribution in Compounds of An Element with A Nearly Full 4d Shell. *Phys. Rev. B* **1985**, *31*, 1903–1908.

48. Zhang, P.; Sham, T. K. Fabrication of Thiol-Capped Pd Nanoparticles: An Electrochemical Method. *Appl. Phys. Lett.* **2003**, *82*, 1778–1780.

49. Sham, T. K. L-Edge X-Ray-Absorption Systematics of the Noble-Metals Rh, Pd, and Ag and the Main-Group Metals In and Sn: A Study of the Unoccupied Density of States in 4d Elements. *Phys. Rev. B* **1985**, *31*, 1888–1902.

50. Coulthard, I.; Sham, T. K. Charge Redistribution in Pd-Ag Alloys from A Local Perspective. *Phys. Rev. Lett.* **1996**, *77*, 4824–4827.

51. Zhang, P.; Sham, T. K. Tuning the Electronic Behavior of Au Nanoparticles with Capping Molecules. *Appl. Phys. Lett.* **2002**, *81*, 736–738.

52. Coulthard, I.; Jiang, D. T.; Lorimer, J. W.; Sham, T. K.; Feng, X. H. Reductive Deposition of Pd on Porous Silicon from Aqueous-Solutions of $PdCl_2$ - An X-Ray-Absorption Fine-Structure Study. *Langmuir* **1993**, *9*, 3441–3445.

53. Wu, Z. B.; Sheng, Z. Y.; Liu, Y.; Wang, H. Q.; Tang, N.; Wang, J. Characterization and Activity of Pd-Modified TiO_2 Catalysts for Photocatalytic Oxidation of NO in Gas Phase. *J. Hazard. Mater.* **2009**, *164*, 542–548.

54. Hsiao, Y. C.; Tseng, Y. H. Preparation of Pd-Containing TiO_2 Film and Its Photocatalytic Properties. *Micro Nano Lett.* **2010**, *5*, 317–320.

55. Vinu, R.; Madras, G. Synthesis and Photoactivity of Pd Substituted Nano-TiO_2. *J. Mol. Catal. A: Chem.* **2008**, *291*, 5–11.

56. Finkelstein, L. D., et al. Band Approach to the Excitation-Energy Dependence of X-Ray Fluorescence of TiO_2. *Phys. Rev. B* **1999**, *60*, 2212–2217.

57. Matsubara, M.; Uozumi, T.; Kotani, A.; Harada, Y.; Shin, S. Polarization Dependence of Resonant X-Ray Emission Spectra in Early Transition Metal Compounds. *J. Phys. Soc. Jpn.* **2000**, *69*, 1558–1565.

58. Higuchi, T., et al. Crystal-Field Splitting and the On-Site Coulomb Energy of $La_xSr_{1-x}TiO_3$ from Resonant Soft-X-Ray Emission Spectroscopy. *Phys. Rev. B* **1999**, *60*, 7711–7714.

Table of Contents (TOC) graphic